Dislocation induced anomalous softening of solid helium

Caizhi Zhou[1,2,*], Jung-Jung Su[1,3], Matthias J. Graf[1], Charles Reichhardt[1], Alexander V. Balatsky[1,3], and Irene J. Beyerlein[1]
[1] *Theoretical Division, Los Alamos National Laboratory, Los Alamos, New Mexico 87545, USA*
[2] *Center for Nonlinear Studies, Los Alamos National Laboratory, Los Alamos, New Mexico 87545, USA*
[3] *Center for Integrated Nanotechnologies, Los Alamos National Laboratory, Los Alamos, New Mexico 87545, USA*
(Dated: October 6, 2011)

The classical motion of gliding dislocation lines in slip planes of crystalline solid helium leads to plastic deformation even at temperatures far below the Debye temperature and can affect elastic properties. In this work we argue that the gliding of dislocations and plasticity may be the origin of many observed elastic anomalies in solid ^{4}He, which have been argued to be connected to supersolidity. We present a dislocation motion model that describes the stress-strain τ-ϵ curves and work hardening rate $d\tau/d\epsilon$ of a shear experiment performed at constant strain rate $\dot{\epsilon}$ in solid helium. The calculated $d\tau/d\epsilon$ exhibits strong softening with increasing temperature due to the motion of dislocations, which mimics anomalous softening of the elastic shear modulus μ. In the same temperature region the motion of dislocations causes dissipation with a prominent peak.

PACS numbers: 61.72.Hh, 67.80.B-, 67.80.bd

The observation of softening of the low-temperature shear modulus in solid ^{4}He with increasing temperature around 100 mK has been taken as evidence for anomalous elastic properties tied to supersolidity [1–4]. Measurements of the shear modulus and the resonant period of torsional oscillator of solid helium showed no period drop in the case of ^{3}He, while both ^{3}He and ^{4}He systems showed softening of the shear modulus in the same temperature range. This result suggested the importance of the role of quantum statistics and the role of defects and moving dislocations on supersolidity [5]. The connection of the motion of dislocations with supersolidity is not certain, whereas the connection of the glide of dislocations with plastic deformation of the crystal is well established [6]. The theory of strain hardening in materials science predicts the stress-strain τ-ϵ curve and allows the study of dislocation motion and plasticity [7, 8]. Such dislocation motion would strongly affect the determination of elastic properties in solid helium, a crystal with a very soft elastic shear modulus [9].

In this Letter, we present a new perspective on the origin of reported anomalous elastic properties of solid helium. The glide of dislocations in a dislocation forest is well understood for typical metals and can lead to large changes of order 60% in the work hardening rate (WHR) [10]. Here, we study the dynamics of classical dislocation motion and plastic behavior of solid helium. At lower temperatures one might expect that quantum dislocation motion will play a significant role [11, 12]. In the case of a DC shear strain rate experiment, $\dot{\epsilon} = const.$, with shear stress τ, we predict the softening of the WHR, $d\tau/d\epsilon$, with increasing temperature T due to dislocation glide and the creation and multiplication of dislocation loops. In the limit of $\epsilon \to 0$ the WHR approaches the elastic shear modulus $d\tau/d\epsilon \to \mu$ and exhibits purely elastic behavior. Our dislocation model also predicts that higher ^{3}He impurity concentration in solid ^{4}He pushes the onset of the magnitude change of $d\tau/d\epsilon$ to higher temperatures, because more ^{3}He atoms pin more dislocations, and the pinning increases the number of immobilized dislocations, causing the crystal to harden. At the same time, the zero-temperature value of the WHR is unaffected by ^{3}He atoms, whereas its high-temperature value is reduced by a lower amount with higher ^{3}He concentrations. Finally, the WHR decreases with increasing strain at finite temperature and attains the elastic shear modulus value at absolute zero temperature.

Our proposed scenario for dislocation dynamics in solid ^{4}He differs from the prevailing view of boiling off of ^{3}He impurities from dislocation lines with increasing T, which act as pinning sites, and the subsequent vibration of longer dislocation segments pinned only by the dislocation network [3, 13–15]. A main result of this work is the prediction of a dissipation peak caused by plastic deformation of the solid in the same temperature region where $d\tau/d\epsilon$ changes most rapidly. All model predictions are remarkably similar to existing shear measurements with applied AC strain rate [1–5] and will provide a stringent test for DC strain rate experiments of solid helium.

We model the elastic and plastic properties of a polycrystalline sample of ^{4}He in the presence of a uniform applied shear stress τ_{app} (see Fig. 1(a)). Plastic deformation arises when the dislocations in the solid start to glide. In the present model, we adopt a statistical representation of a group of dislocations, which neglects individual dislocation characteristics such as polarity, line orientation, etc. The dislocation network is then represented by a continuous distribution of dislocations and characterized by a linear density ρ (total length of dislocation lines over the sample volume). The *total* dislocation density in a material consists of both *mobile* and *stored* (immobile) dislocations

$$\rho_{tot} = \rho_{mob} + \rho_{stored}. \quad (1)$$

Immobile dislocations may be glissile, that is, pinned by

defects, or sessile, that is, lying out of their habit plane. For example, glissile dislocations can be pinned when decorated with ^{3}He atoms as sketched in Fig. 1(b). Both ρ_{mob} and ρ_{stored} evolve as deformation proceeds.

During the time Δt glide increases the total dislocation density according to [8]

$$\Delta\rho_{tot} = \beta\rho_{mob}\, v\Delta t/L, \tag{2}$$

where $L \sim 1/\sqrt{\rho_{tot}}$ is the mean-free path of the mobile dislocations, v is their average speed, and the geometric coefficient $0 < \beta < 1$ is indicative of how fast the density increases as dislocation loops propagate [8]. The increments in stored and mobile dislocation densities are generally proportional to $\Delta\rho_{tot}$, as portions of an expanding dislocation loop can react with other loops and become permanently immobilized. Combining Eqns. (1) and (2), we arrive at $\Delta\rho_{mob} = c\Delta\rho_{tot}$ and $\Delta\rho_{stored} = (1-c)\Delta\rho_{tot}$, with $0 < c < 1$.

For simplicity, we assume an average speed v for all mobile dislocations in the sample volume and that their speeds are sufficiently low, such that their motion is controlled by thermal activation obeying an Arrhenius law. In this regime, mobile dislocations glide from one pinning point (^{3}He or intersecting dislocations) to another. Their motion is resisted by τ_{res}, however, a combination of thermal energy and mechanical work in excess of τ_{res} can overcome the Gibb's free energy of activation, $\Delta G = U_i - \tau_{eff}V$, with effective stress $\tau_{eff} = \tau_{app} - \tau_{res}$ and activation volume V. Accordingly, the average dislocation speed as a function of stress and temperature is given by [7, 8]

$$v = b\nu_D \exp\left[-\Delta G/k_BT\right]. \tag{3}$$

The magnitude of the Burgers vector is $b = |\mathbf{b}|$, the Debye frequency is ν_D, the pinning energy is U_i, and the active volume is $V = b^2\, L$. We model the resistance stress by [7, 8]

$$\tau_{res} = \tau_{Peierls} + \alpha\mu b\sqrt{\rho_{tot}}, \tag{4}$$

with Peierls stress $\tau_{Peierls}$, elastic shear modulus μ, and typical coefficient $0.1 < \alpha < 2$ [16]. In mean-field theory, the second term in (4) arises due to long-range interactions with other dislocations in the background.

The total applied strain is accommodated by both elastic and plastic strain, $\epsilon_{tot} = \epsilon_e + \epsilon_p$. The plastic strain rate due to glide obeys [6]

$$\dot{\epsilon}_p = bv\,\rho_{mob}. \tag{5}$$

The corresponding applied shear stress τ_{app} follows Hooke's law and obeys

$$\tau_{app} \equiv \mu\epsilon_e = \mu\big(\epsilon_{app} - \epsilon_p\big). \tag{6}$$

Since the plastic work W_p equals $\tau_{app}\,\epsilon_p$, one should note that dislocation glide yields a finite plastic strain rate $\dot{\epsilon}_p$ that gives rise to finite dissipation ($\dot{W}_p$).

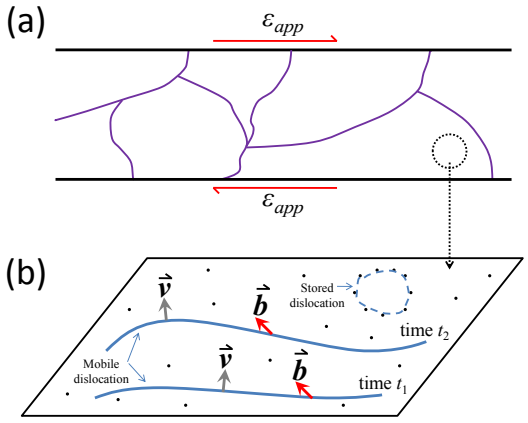

FIG. 1: (Color online). (a) Illustration of the applied shear stress on the solid ^{4}He sample with curved lines indicating grain boundaries; (b) magnification of circled region in (a) and plot of a mobile dislocation moving on the slip plane under external load. Black dots indicate ^{3}He pinning points, solid lines are mobile dislocations, and dashed lines are stored (immobile) dislocations.

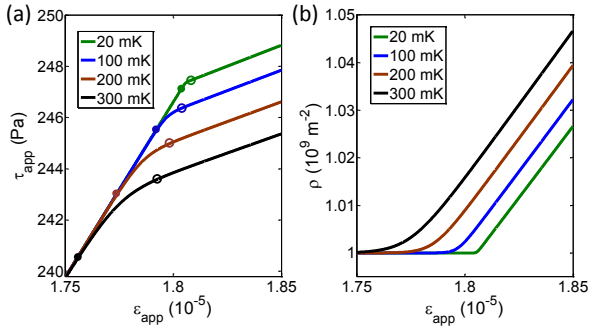

FIG. 2: (Color online). (a) Stress-strain curves for different temperatures at applied strain rate $\dot{\epsilon} = 0.1$ s^{-1} with initial total and mobile dislocation densities 10^9 m^{-2} and 10^8 m^{-2}, respectively. The filled and open circles bracket the transition zone between elastic and plastic behavior. (b) Plot of the corresponding dislocation density-strain curves of (a). As temperature decreases, the transition point is delayed to higher shear strain and the transition zone narrows and sharpens.

The stress-strain curves in Fig. 2(a) show plastic behavior (deviation from the linear stress-strain curve) above a critical applied strain. The transition zone from elastic to plastic behavior is indicated by filled and open circles along the stress-strain curves. The applied stress effectively lowers the barrier given by the Gibb's free energy $\Delta G = U_i + \tau_{res}V - \tau_{app}V$. When $\tau_{app} < \tau_c$ only a negligible amount of the dislocations can thermally overcome the "effective" barrier. The dislocation lines are essentially pinned and the sample remains elastic. When $\tau_{app} > \tau_c$ an increasing amount of dislocations starts to glide, which produces plastic strain ϵ_p for the same applied stress (deviation from elastic behavior). Accordingly dislocation loops grow in size, thus increasing the dislocation density shown in Fig. 2(b). Tempera-

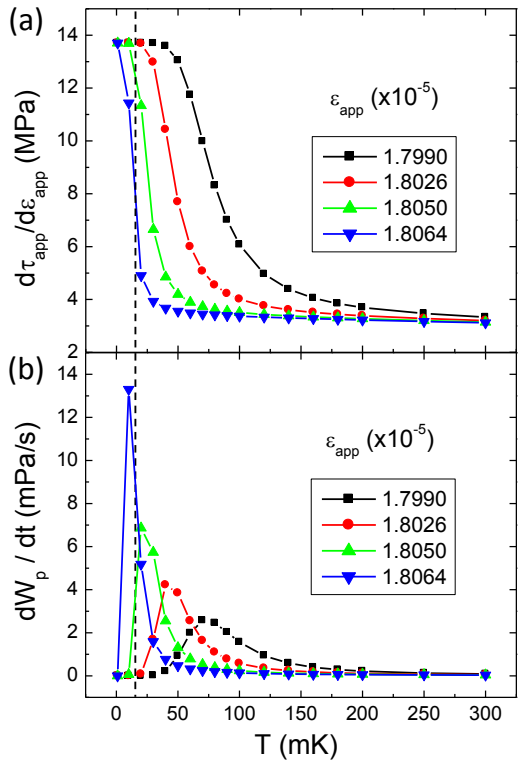

FIG. 3: (Color online). (a) Work hardening rate versus temperature for different strains. The parameters are the same as in Fig. 2; (b) corresponding plastic dissipation of (a). The dashed line at $T = 20$ mK marks the cutoff of a typical low temperature experiment. For thermally activated dislocation glide the work hardening rate approaches the elastic shear modulus at $T = 0$ K and no plastic work is dissipated.

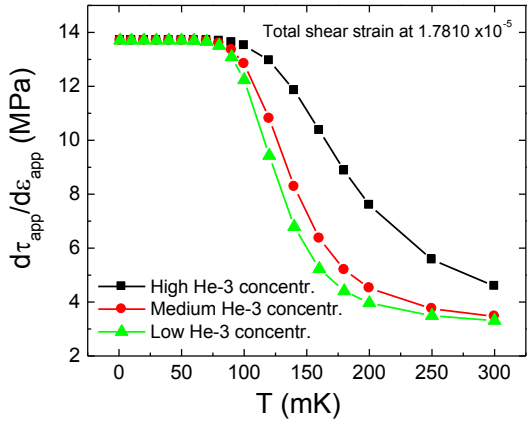

FIG. 4: (Color online). Work hardening rate versus temperature for different pinning point (^{3}He) concentrations. The curves for high, medium, low ^{3}He concentrations correspond to initial mobile dislocation densities of $1\times10^8, 5\times10^8, 9\times10^8$ m^{-2}, respectively. All calculations have the same initial total dislocation density of 10^9 m^{-2} and total strain amplitude $\epsilon = 1.7810 \times 10^{-5}$ [28].

ture comes into play in the elastic-plastic cross-over, since our model describes dislocation gliding as a thermally activated process in Eq. (3): At higher temperature, more dislocations can overcome the barriers. This corresponds to a lower critical strain and broader transition shown in Fig. 2(a) at high temperature. The dislocation density then increases at a lower applied stress (strain) displayed in Fig. 2(b). In the calculation shown here and after we take the pinning potential U_i to be set by the Debye temperature $\Theta_D = 28.8$ K [17, 18], since we postulate that pinning originates from dislocation crossing or local melting. Most materials parameters have been reported in the literature: $b = 0.364$ nm, $\mu = 13.7$ MPa [19], $\tau_{Peierls} = 10^{-5}\,\mu$ [20]. The fundamental results in this study are not sensitive to the assumed model parameters, such as $\alpha = 0.1$, $\beta = 0.9$ and $c = 0.5$.

The slope of the stress-strain curve defines the work hardening rate (WHR$\equiv d\tau_{app}/d\epsilon_{app}$). The WHR and dissipation in Fig. 3 show a decrease in the WHR above ~ 100 mK accompanied by a dissipation peak. This result is strikingly similar to measurements of the dynamic shear modulus. At low temperature the WHR is the value of an ideal crystal with no dissipation, since dislocation glide is negligible. At the crossover temperature, dislocations start to overcome barriers and glide. Dislocation glide contributes additional strain, which reduces the WHR while simultaneously dissipating energy giving rise to a dissipation peak. At even higher temperatures, dislocation lines are essentially free to glide viscously; the system exhibits plastic strain but dissipates only minimal energy. We also show the WHR and dissipation for different applied strains in Fig. 3. The crossover temperature for a larger applied stress (strain) is lower since the "effective barrier" is lower in that case.

Our dislocation glide model can capture the effect of ^{3}He impurities as well. We propose that ^{3}He atoms decorating dislocation lines exert a drag on moving dislocations, instead of pinning them since dissolved ^{3}He atoms exhibit a very high mobility in solid ^{4}He compared to the speed of dislocations. We model a lower ^{3}He concentration by a higher initial mobile density ρ_{mob} and vice versa for the same initial total dislocation density. Fig. 4 shows the WHR versus temperature. The curves for high, medium, low ^{3}He concentrations correspond to initial mobile dislocation densities of $1\times10^8, 5\times10^8, 9\times10^8$ m^{-2}, respectively. When the ^{3}He concentration is low, the main obstacle for dislocation gliding is still the Peierls potential and the background interaction. Hence the result does not depend much on the ^{3}He concentration. When the ^{3}He concentration is high enough, the viscous drag starts to dominate over other effects and causes a broader crossover at higher temperatures. This is in accordance with the observations made in various experiments and shown for low, medium, and high ^{3}He concentrations in Fig. 4.

We next discuss the similarities and differences between our calculations and the previous AC strain measurements of the dynamic shear modulus [1–3]. Although we model an applied DC strain rate measurement, the

results share the same qualitative features with the AC experiment: both show decreases in the WHR above a crossover temperature accompanied by a dissipation peak. However, the magnitudes of these features between our theory and measurements are quite different. Large differences in stress-strain relations have been reported before between free-standing and confined crystals of solid helium and may be a contributing factor to this discrepancy [21]. The critical strain in the AC experiment is about 10^{-7}, while in our model it is roughly 10^{-5}. The ratio of change in the WHR is also much smaller in the AC measurement ($\sim 15\%$) than in this calculation ($\sim 60\%$). This suggests that the AC experiment may measure a type of dislocation motion that dissipates less energy than gliding. In particular this motion should not involve moving the entire dislocation line from one Peierls valley to another, since the critical stress in the AC measurement ($\tau_c \sim 10^{-7}\mu$) is at least two orders of magnitude smaller than the Peierls stress ($\tau_{Peierls} > 10^{-5}\mu$). A potential explanation for such motion includes dislocation vibration [13] and kink motion [22, 23]. If this mechanism can be proven dominant, then the dislocation motion is different in the AC and DC strain rate experiments and may resolve the inconsistencies between the torsional oscillator (TO) results with and without a rotating DC component [24]. In this case, our dislocation glide model may be generalized to include dislocation vibration at low strains to explain the AC shear modulus and TO experiments with a superimposed DC rotation.

Finally we note that grain boundaries and the distribution of multiple grain orientations can change the strength of the effect. In a polycrystalline system, the strain from different grains can act along different directions and partially cancel each other out. This would diminish the observed effect. Indeed ultrasound measurements observed a smaller change in the shear modulus of polycrystalline samples compared to single crystals. For high quality single crystals a change of 86% was reported [4]. Our model does not include such cancellation effects. This may partly explain why the AC strain rate measurement in polycrystals observes a smaller effect.

In summary, we proposed a simplified isotropic density-based dislocation model to describe qualitatively many essential features of the anomalous low-temperature shear modulus of solid ^{4}He measured with an AC strain rate. More importantly, we predicted many new stress-strain curves, work hardening rates, and dissipation properties for a DC strain rate shear experiment. In our model, the classical glide of dislocations in slip planes under load has no relationship with supersolidity.

One may speculate that the existence and dominance of dislocation induced plastic deformation facilitates a nonuniform supersolid state, because a supersolid state is possible in ^{4}He along the core of static dislocations [25, 26]. An interesting aspect of a highly tangled dislocation network may be its local loss of crystalline order, due to strong lattice distortions by closely arranged dislocation cores [27]. Those distorted regions are more amenable for superfluidity and are a potential candidate for a nonuniform supersolid phase. The dynamic effects of plastic deformations and dislocation glide discussed here will play a role in the dynamic measurements of solid ^{4}He regardless of the presence or absence of superfluidity. In the absence of more detailed microstructural information the model proposed here offers an effective method to check whether the dislocation motion is the fundamental mechanism for plasticity in solid helium.

We acknowledge discussions with J. Beamish and C. J. Olson-Reichhardt. This work was supported by the U.S. DOE at Los Alamos National Laboratory under contract No. DE-AC52-06NA25396 and the Office of Science (BES). CZ acknowledges support provided by the Center for Nonlinear Studies, Statistical Physics Beyond Equilibrium Project from the Los Alamos National Laboratory Directed Research and Development Office. * czhou@lanl.gov

[1] J. Day and J. Beamish, Nature **150**, 853 (2007).
[2] J. Day, O. Syshchenko and J. Beamish, Phys. Rev. B **79**, 214524(2009).
[3] O. Syshchenko, J. Day, and J. Beamish, Phys. Rev. Lett. **104**, 195301 (2010).
[4] X. Rojas et al., Phys. Rev. Lett. **105**, 145302 (2010).
[5] J. T. West et al., Nature Physics **5**, 598 (2009).
[6] E. Orowan, Proc. Phys. Soc. **52**, 8 (1940).
[7] U. F. Kocks, A. S. Argon, and M. F. Ashby, Prog. Mater. Sci. **19**, 1 (1975).
[8] U. F. Kocks and H. Mecking, Prog. Mater. Sci. **48**, 171 (2003).
[9] M. A. Paalanen, D. J. Bishop, and H. W. Dail, Phys. Rev. Lett. **46**, 664 (1981).
[10] B. Wielke, phys. stat. sol. (a) **33**, 241 (1976).
[11] N. F. Mott, Philos. Mag. **1**, 568 (1956).
[12] J. J. Gilman, J. App. Phys. **39**, 6086 (1968).
[13] A. Granato and K. Lücke, J. Appl. Phys. **27**, 583 (1956).
[14] I. Iwasa and H. Suzuki, J. Phys. Soc. Jpn. **49**, 1722 (1980).
[15] I. Iwasa, Phys. Rev. B **81**, 104527 (2010).
[16] I. J. Beyerlein and C. N. Tome, Int. J. Plasticity **24**, 867 (2008).
[17] D. O. Edwards and R. C. Pandorf, Phys. Rev. **140**, A816 (1965).
[18] D. S. Greywall, Phys. Rev. B **16**, 5127 (1977).
[19] H. Suzuki, J. Phys. Soc. Jpn. **42**, 1865 (1977).
[20] Y. Hiki, and F. Tsuruoka, Phys. Rev. B **27**, 696 (1983).
[21] D. J. Sanders et al., Phys. Rev. Lett. **39**, 815 (1977).
[22] P.-G. de Gennes, C. R. Physique **7**, 561, (2006).
[23] D. Aleinikava et al., Euro. Phys. Letts. **89**, 46002 (2010).
[24] H. Choi et al., Science **330**, 1512 (2010).
[25] M. Boninsegni *et al.*, Phys. Rev. Lett., **99**, 035301 (2007).
[26] S. Balibar, Nature (London) **464**, 176 (2010).
[27] C. Suryanarayana, Prog. Mater. Sci. **46**, 1 (2001).
[28] See EPAPS Document x.